

Intermediate-valence icosahedral Au-Al-Yb quasicrystal

Tetsu Watanuki,^{1,*} Shiro Kashimoto,² Daichi Kawana,^{1,†} Teruo Yamazaki,^{3,‡}
Akihiko Machida,¹ Yukinori Tanaka,² and Taku J. Sato^{3,§}

¹Condensed Matter Science Division, Quantum Beam Science Directorate, Japan Atomic Energy Agency, Sayo, Hyogo 679-5148, Japan

²Graduate School of Engineering, Hokkaido University, Sapporo 060-8628, Japan

³Neutron Science Laboratory, Institute for Solid State Physics, University of Tokyo, 106-1 Shirakata, Tokai, Ibaraki 319-1106, Japan

(Received 19 August 2011; revised manuscript received 4 July 2012; published 10 September 2012)

A quasiperiodic intermediate-valence (IV) system is realized in an icosahedral Au-Al-Yb quasicrystal. X-ray absorption spectroscopy near the Yb L_3 edge indicates that quasiperiodically arranged Yb ions assume a mean valence of 2.61, between a divalent state ($4f^{14}$, $J = 0$) and a trivalent one ($4f^{13}$, $J = 7/2$). Magnetization measurements demonstrate that the $4f$ holes in this quasicrystal have a localized character. The magnetic susceptibility shows a Curie-Weiss behavior above ~ 100 K with an effective magnetic moment of $3.81\mu_B$ per Yb. Moreover, a crystalline approximant to this quasicrystal is an IV compound. We propose a heterogeneous IV model for the quasicrystal, whereas the crystalline approximant is most likely a homogeneous IV system. At temperatures below ~ 10 K, specific heat and magnetization measurements reveal non-Fermi-liquid behavior in both the quasicrystal and its crystalline approximant without either doping, pressure, or field tuning.

DOI: [10.1103/PhysRevB.86.094201](https://doi.org/10.1103/PhysRevB.86.094201)

PACS number(s): 61.44.Br, 75.50.Kj, 75.30.Mb, 78.70.Dm

Intermediate valence (IV) compounds are attractive due to their charge degree of freedom. Their electrons have the potential to exhibit either an itinerant or localized character. For example, IV $4f$ -electron systems such as rare-earth-based crystalline compounds show diverse physical properties that depend on the itinerant or localized $4f$ -electron character. Various phenomena have been observed such as valence fluctuation, heavy fermions, non-Fermi-liquid behavior, superconductivity, charge ordering, and complex magnetic ordering.¹

There is a great deal of interest in realizing quasicrystalline IV systems because this is expected to result, for example, in a valence fluctuation state in a quasiperiodic system with itinerant $4f$ character, or a quasiperiodic charge order or a charge glass with localized $4f$ character. Moreover, the research field of heavy fermions will be extended to quasiperiodic systems. The Ruderman-Kittel-Kasuya-Yosida-Kondo (RKKY-Kondo) competition in quasicrystals has already been studied vigorously in Al-Pd-Mn alloys,² but they have been restricted to a dilute-Kondo system. However, quasicrystalline IV compounds, where IV $4f$ ions form a quasiperiodic lattice, correspond to the quasi-periodic Anderson model, in which the lattice structure should be more influential. In our previous studies, we have demonstrated quasiperiodic IV systems by applying pressure to Cd-Yb (Ref. 3) and Cd-Mg-Yb (Ref. 4) icosahedral quasicrystals.⁵⁻⁷ Although the Yb ions show a divalent form in these quasicrystals, pressure converts them to a noninteger valence, an IV state between divalent ($4f^{14}$) and trivalent ($4f^{13}$). The Yb valence increases continuously upon compression, and for a Cd-Mg-Yb quasicrystal, the valence reaches 2.71 at 57.6 GPa.⁷ However, IV quasicrystals at ambient pressure have yet to be found.

Recently, Ishimasa *et al.* have synthesized a candidate material that could lead to IV quasicrystals at ambient pressure.⁸ An $\text{Au}_{51}\text{Al}_{34}\text{Yb}_{15}$ icosahedral quasicrystal (*i*-AuAlYb) belongs to Tsai-type quasicrystals⁹ as well as Cd-Yb and Cd-Mg-Yb icosahedral quasicrystals that consist of Tsai-type atomic clusters (Fig. 1) with a quasiperiodic arrangement.^{8,10} Although the structural analysis on *i*-AuAlYb has not yet been carried out,

it is possible to construct a crude structure model (Fig. 1) by referring to the refined structures of the Cd-Yb quasicrystal¹⁰ and the 1/1 cubic crystalline approximant (*c*-AuAlYb) (Ref. 8) to *i*-AuAlYb. Basically, the Cd atom in the Cd-Yb quasicrystal is replaced by Au-Al. The Yb ions occupy two types of specific sites: the major one (site *A*) is located at the second shell of the atomic cluster, where 12 Yb ions form an icosahedron (Fig. 1), and the minor one (site *B*) is in the gaps of the cluster packing.¹⁰ The population ratio of sites *A* to *B* is approximately 7:3.¹¹ Thus, a quasiperiodic Yb lattice is constructed without chemical disorder. According to Ref. 8, the Yb ions in *i*-AuAlYb may exhibit the IV state. Specifically, using the relationship between the atomic radius of the second shell element and the six-dimensional lattice constant of the quasicrystal, the estimated Yb ionic radius in *i*-AuAlYb is an intermediate value between the divalent and trivalent ones.

Herein, we use x-ray absorption spectroscopy and magnetization measurements to demonstrate the realization of a quasiperiodic IV system in *i*-AuAlYb and the localized character of the $4f$ -electron system in *i*-AuAlYb, respectively. Moreover, a periodic counterpart to *i*-AuAlYb, i.e., *c*-AuAlYb, is shown to be an IV compound.

We began by preparing an alloy with the nominal composition of $\text{Au}_{49}\text{Al}_{34}\text{Yb}_{17}$ from high-purity materials [Au (purity, 99.99 wt%), Al (purity, 99.999 wt%), and Yb (purity, 99.9 wt%)] in an arc furnace with an argon atmosphere. The as-cast specimen was identified as *i*-AuAlYb with a six-dimensional lattice parameter $a_{6D} = 7.448(2)$ Å by an x-ray diffraction measurement using Cu $K\alpha$ radiation. Electron probe microanalysis indicated that the composition was $\text{Au}_{51}\text{Al}_{34}\text{Yb}_{15}$, which is the same value as in Ref. 8. The small difference between the nominal and analyzed compositions is mainly due to evaporation of Yb during the alloying. Another alloy with a nominal composition of $\text{Au}_{49}\text{Al}_{36}\text{Yb}_{15}$ was prepared by a similar method, but was subsequently annealed at 700 °C for 24 h. The specimen with an analyzed composition of $\text{Au}_{51}\text{Al}_{35}\text{Yb}_{14}$ was assigned to *c*-AuAlYb.⁸

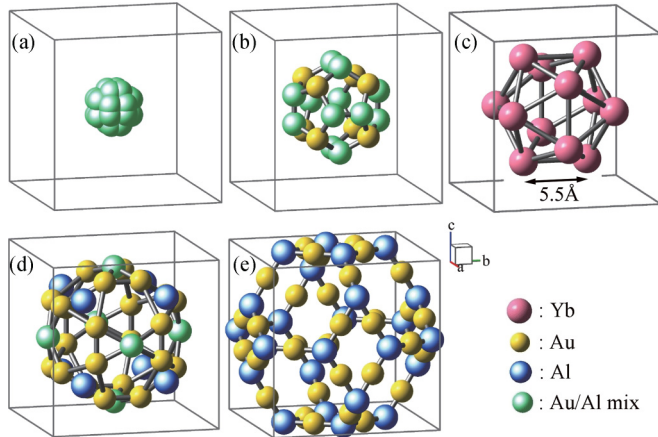


FIG. 1. (Color online) Illustration of a Tsai-type atomic cluster in an $\text{Au}_{51}\text{Al}_{34}\text{Yb}_{15}$ icosahedral quasicrystal (*i*-AuAlYb) and its 1/1 crystalline approximant of $\text{Au}_{51}\text{Al}_{35}\text{Yb}_{14}$ (*c*-AuAlYb). Each cluster consists of a concentric arrangement of triple shells, i.e., 20 Au/Al dodecahedron (b), 12 Yb icosahedron (c), and 30 Au/Al icosidodecahedron (d). The cluster center is filled with orientationally disordered 4 Au/Al atoms (a). For *c*-AuAlYb, the clusters are embedded in a cage network as shown in (e). For details, see Ref. 8.

We measured the Yb valence of *i*-AuAlYb at room temperature by Yb L_3 -edge x-ray absorption near-edge structure (XANES) spectroscopy in BL22XU at SPring-8.¹² The 40- μm -diameter collimated monochromatic x-ray beam was directed at the center of a cracked $90\ \mu\text{m} \times 90\ \mu\text{m} \times 15\ \mu\text{m}$ piece, which consisted of several single-quasicrystal domains, of the alloy ingot. Transmission XANES spectra were acquired by scanning the incident x-ray energy between 8.77 and 9.11 keV using two ionization chambers filled with N_2 gas to monitor the incident and transmitted x-ray intensities. We measured *c*-AuAlYb in a similar manner. The dc magnetization measurements were performed on both *i*-AuAlYb and *c*-AuAlYb between 2 and 300 K in a 600-Oe field, using a superconducting quantum interference device (SQUID) magnetometer (Quantum Design, MPMS 7 and MPMS XL-7). Additionally, specific heats of both *i*-AuAlYb and *c*-AuAlYb were measured by a thermal relaxation method at low temperatures between 0.38 and 20 K in a zero magnetic field, and below 10 K in 35- and 70-kOe fields, using a Quantum Design physical property measurement system with a ^3He option.

Figure 2(a) shows the normalized XANES spectrum of *i*-AuAlYb, where the absorption edge obviously exhibited a double peak. The lower energy peak around 8.939 keV corresponds to the divalent component, while the higher one around 8.946 keV corresponds to the trivalent one. The results indicate that an IV state is realized in *i*-AuAlYb. The mean valence was determined using the same procedure as in our previous paper.⁵ As shown in Fig. 2(a), the spectrum is well fitted by the sum of the divalent $S_{\text{div}}(E)$ and trivalent $S_{\text{tri}}(E)$ components $(1-x)S_{\text{div}}(E) + xS_{\text{tri}}(E)$. The mean valence was obtained from $\bar{v} = x + 2$, $\bar{v} = 2.61(4)$. Because divalent Yb has a filled $4f^{14}$ shell ($J = 0$), but trivalent Yb of the $4f^{13}$ state ($J = 7/2$) contains one hole, the hole density n_h (4*f*-hole number per Yb site) is 0.61 due to the relation $n_h = v - 2$. For Yb-based IV crystalline compounds, as the 4*f*-hole density increases, the 4*f* hole-hole correlation becomes stronger and

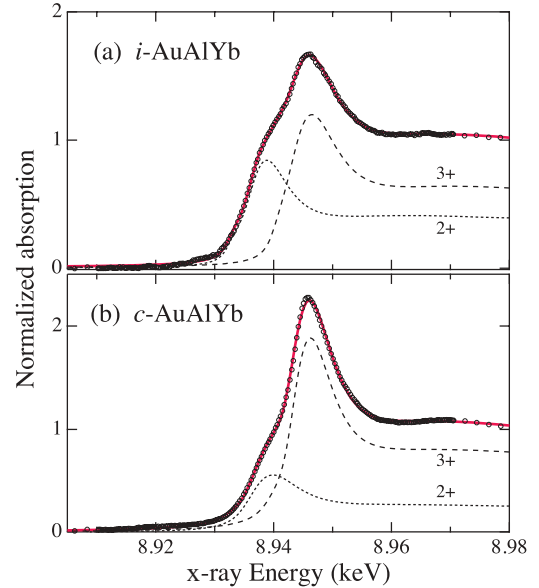


FIG. 2. (Color online) Normalized Yb L_3 XANES spectra of *i*-AuAlYb (a) and *c*-AuAlYb (b) at room temperature (open circles). Normalization is applied so that the higher-energy data up to 9.11 keV asymptotically approaches a unit. Each spectrum is fitted by the sum (solid red line) of the divalent (dotted line) and trivalent (dashed line) components.

the behavior of 4*f* holes changes from itinerant to localized. The boundary between itinerant and localized is around n_h of 0.7 ($v \sim 2.7$).^{6,7,13} The value of $n_h = 0.61$ suggests that the 4*f* system of *i*-AuAlYb is in the itinerant region but near the boundary between itinerant and localized states.

To determine whether the 4*f* holes exhibit an itinerant or localized character, we performed magnetization measurements. For the itinerant case, the magnetic susceptibility gives almost temperature-independent behavior, whereas localized magnetic moments appear in the localized case. It should be noted that XANES can not distinguish between these two cases because of using an optical process with a fast time scale of $\sim 10^{-16}$ s. Figure 3(a) shows the inverse plot of the temperature dependence of the magnetic susceptibility $\chi(T)$ of *i*-AuAlYb. Above ~ 100 K, the magnetic susceptibility is characterized by a Curie-Weiss behavior, and $\chi(T)$ is well fitted by $\chi(T) = C/(T - \theta_p) + \chi_0$, where C is the Curie constant, θ_p is the paramagnetic Curie temperature, and χ_0 is a constant term. The calculated effective magnetic moment μ_{eff} per Yb site from the Curie constant is $3.81\mu_B$, the θ_p is -138 K, and the χ_0 is -1.4×10^{-4} emu/mol-Yb. The negative value of χ_0 is due to the core diamagnetism of *i*-AuAlYb, -2.6×10^{-4} emu/mol-Yb.

These results indicate that the 4*f* holes have a localized character, where the magnetic moment appears. Compared to the trend of Yb-based IV crystalline compounds, a valence of 2.61 is rather low for displaying a localized character. For example, Yb valence of YbCu_4Ga , $v = 2.59$ at 300 K, is similar to that of *i*-AuAlYb, but the $\chi(T)$ is much suppressed from a Curie-Weiss model and shows almost temperature-independent behavior, indicating itinerant 4*f* character.^{14,15} The reasons for the localized 4*f* character in *i*-AuAlYb are discussed later.

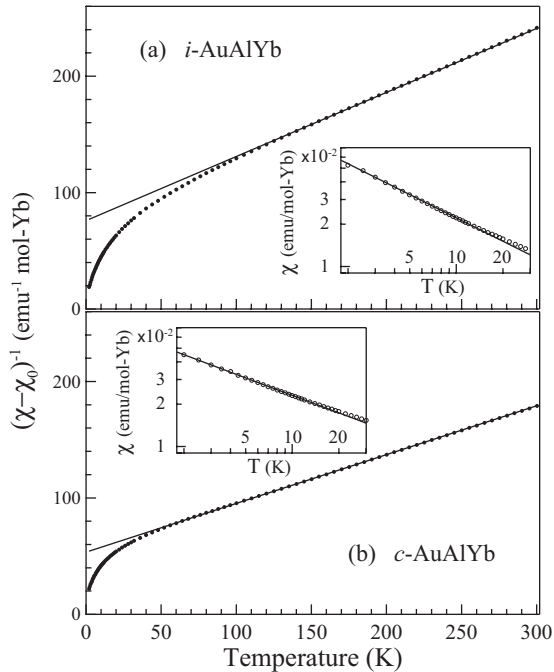


FIG. 3. Inverse plots of magnetic susceptibility of *i*-AuAlYb (a) and *c*-AuAlYb (b) as a function of temperature (closed circles). Solid lines denote Curie-Weiss fits. Insets are logarithm plots of the $\chi(T)$'s in the low-temperature region (open circles). Solid lines are fits to the power law.

The periodic counterpart to *i*-AuAlYb is *c*-AuAlYb, which consists of the same Tsai-type atomic cluster as *i*-AuAlYb, but in a different arrangement, i.e., the bcc packing structure [$a_0 = 14.500(2)$ Å], where all the Yb sites belong to site A and are crystallographically equivalent (Fig. 1).^{8,10} Hence, *c*-AuAlYb is expected to have an IV state. Thus, the Yb valence was measured at room temperature by XANES spectroscopy. Figure 2(b) shows the normalized XANES spectrum of *c*-AuAlYb. The double-peak structure is again observed in the absorption edge, indicating that the Yb ions assume an IV state. The mean valence is 2.80(5), which is higher than that of *i*-AuAlYb. We also performed magnetization measurements, and Fig. 3(b) shows the $\chi(T)$ of *c*-AuAlYb. Similar to *i*-AuAlYb, $\chi(T)$ of *c*-AuAlYb displays a Curie-Weiss behavior above ~ 50 K, with μ_{eff} , θ_p , and χ_0 of $4.37\mu_B$, -127 K, and -8.1×10^{-4} emu/mol-Yb, respectively. The result indicates that the $4f$ holes in *c*-AuAlYb show a localized character, as in the case of *i*-AuAlYb. However, unlike the case of *i*-AuAlYb, the localized character with the valence of 2.8 is consistent with the trend of Yb-based IV compounds. The rather large negative value of χ_0 is presumably due to the diamagnetic orbital contributions in addition to the core diamagnetism, as in the case of Al-based quasicrystals containing Mn.²

The two compounds (*i*-AuAlYb and *c*-AuAlYb) exhibit similar characters in the higher-temperature region above ~ 100 K. This result is attributed to similarities in their local structures. The Yb valence value mainly depends on the local structure around the Yb ion, and magnetic susceptibility in the high-temperature regime reflects the short-range character. Nevertheless, the difference of their Yb character should be further investigated: μ_{eff} of $3.81\mu_B$ in *i*-AuAlYb is obviously

smaller than $\mu_{\text{eff}}[\text{Yb}^{3+}]$ of $4.54\mu_B$, whereas the μ_{eff} of $4.37\mu_B$ in *c*-AuAlYb is close to the $\mu_{\text{eff}}[\text{Yb}^{3+}]$, where $\mu_{\text{eff}}[\text{Yb}^{3+}]$ is the effective magnetic moment for the free trivalent Yb ion. The difference between their μ_{eff} values implies a certain difference between their Yb characters.

First, we investigated the Yb character of *c*-AuAlYb. Because each Yb is crystallographically equivalent,⁸ every Yb site is considered to have a homogeneous mean valence of 2.80. This consideration is consistent with the observed $|\theta_p|$ over 100 K, which is much higher than the typical magnetic transition temperature of several Kelvin¹⁶ due to the RKKY interaction for Yb-based intermetallic compounds. Since $|\theta_p|$ roughly corresponds to Kondo temperature (T_K) for IV *f*-electron compounds,¹⁵ the observed high $|\theta_p|$ indicates a large conduction (*c*)-*f* exchange coupling J_{cf} that causes screening of the magnetic moments by conduction electrons. For homogeneous IV Yb-based compounds, $|\theta_p|$ sensitively increases with decreasing valence because screening increases with increasing the proportion of nonmagnetic divalent component at each Yb site. This relationship is clearly seen in the sequential system such as $\text{YbCu}_{5-x}\text{Al}_x$, where $|\theta_p|$ of 20 K at the valence of 2.97 ($x = 2$) reaches 350 K at the valence of 2.85 ($x = 1$).^{17,18} As for the temperature scale, $|\theta_p|$ of ~ 100 K (neither several Kelvin range nor much higher temperature scale than the room temperature) is typically observed around the valence of 2.8, as seen in the $\text{YbCu}_{5-x}\text{Al}_x$ system and as also reported in YbAl_3 of $\theta_p = -225$ K (Ref. 19) or YbPd of $\theta_p = -95.5$ K (Ref. 20) at their valence of 2.8.^{20,21} Thus, the relationship between valence of 2.80 and $\theta_p = -127$ K in *c*-AuAlYb is in accordance with the typical cases of homogeneous IV Yb-based compounds. The observed slightly smaller μ_{eff} value than $\mu_{\text{eff}}[\text{Yb}^{3+}]$ can be attributed to the screening effect.

As for the crystal electric field (CEF) effect, $1/\chi(T)$ shows nonlinear temperature dependence below the temperature scale of CEF energy but above the temperature $1/\chi(T)$ asymptotically approaching to Curie-Weiss behavior. Therefore, the CEF effect is negligible in these arguments that treat the temperature region where Curie-Weiss character is clearly exhibited. Moreover, the obtained μ_{eff} value is close to the $\mu_{\text{eff}}[\text{Yb}^{3+}]$, which again indicates that the temperature scale in this region exceeds the CEF split energy.

Next, we investigated *i*-AuAlYb for which, unlike for *c*-AuAlYb, the homogeneous IV picture gives inconsistencies as follows: each Yb site in *i*-AuAlYb is interpreted to contain divalent component in the proportion of 0.39, which is approximately double compared to 0.20 for *c*-AuAlYb. Therefore, $|\theta_p|$ of *i*-AuAlYb should much higher than that of *c*-AuAlYb. In actuality, however, the θ_p of *i*-AuAlYb is close to that of *c*-AuAlYb. This discrepancy is related to the previous remark, that is, homogeneous IV Yb-based compounds with similar valence to *i*-AuAlYb show itinerant $4f$ character, which indicates that their T_K 's are sufficiently higher than room temperature and, consequently, the temperature scale is much different from the θ_p of *i*-AuAlYb. In addition, the $\chi(T)$ behavior in *i*-AuAlYb is not consistent with the homogeneous IV picture in which the $\chi(T)$ is phenomenologically described by the interconfiguration fluctuation (ICF) model. According to this model, the Curie constant (C) is replaced by a temperature-dependent term, i.e.,

$C \propto 8/[8 + \exp\{-E_{\text{ex}}/k_{\text{B}}(T + T_{\text{sf}})\}]$, where E_{ex} is energy difference between the $4f^{14}$ and $4f^{13}$ states, and T_{sf} is the fluctuation temperature.²² A larger temperature dependence is seen as the divalent component increases, as shown in the reports on $\text{YbCu}_{5-x}\text{Al}_x$ and $\text{YbCu}_{5-x}\text{Ga}_x$.^{15,17} However, C of $i\text{-AuAlYb}$ does not show such a temperature dependence, but instead exhibits a normal Curie-Weiss constant character, despite the comparatively large proportion of the divalent component. We unsuccessfully tried to fit $\chi(T)$ of $i\text{-AuAlYb}$ using an ICF model with the constraint of $\nu = 2.61$ at 300 K.

We, therefore, propose a heterogeneous valence model for $i\text{-AuAlYb}$; that is, the major Yb sites assume a high valence with a magnetic moment similar to $c\text{-AuAlYb}$, and the remaining minor sites exhibit a low valence and nonmagnetic state. According to this model, the high-valence Yb ions account for the similarity of the θ_p value to that of $c\text{-AuAlYb}$ and also for the Curie-Weiss character of $\chi(T)$. In addition, the smaller μ_{eff} in $i\text{-AuAlYb}$ than that in $c\text{-AuAlYb}$ is explained by the average of these two sites. $i\text{-AuAlYb}$ may lead to such heterogeneous-valence structure because of containing two types of Yb sites with different local structures (sites A and B). Additionally, charge disproportionation should be promoted because electrons in quasicrystals tend to be localized.²³ It is reasonable to expect site A in $i\text{-AuAlYb}$ to have a valence and a magnetic moment close to those of $c\text{-AuAlYb}$ because of the similarity in the local structure. Assuming that site A in $i\text{-AuAlYb}$ has the same values as those in $c\text{-AuAlYb}$, the valence at site B is calculated to be 2.19 by employing the population ratio of sites A to B . This valence value suggests nonmagnetic character of site B because Yb close to divalent typically shows nonmagnetic character such as $\text{Yb}_2\text{Pd}_3\text{Sn}_5$ ($\nu = 2.21$).²⁴ The site averaged μ_{eff} is calculated to be $3.63\mu_{\text{B}}$, which mostly agrees with the experimental result of $3.81\mu_{\text{B}}$. We note that $i\text{-AuAlYb}$ is not a simple mixed integer-valence system of divalent and trivalent ions, but a heterogeneous IV system, where the IV state is exhibited at least at site A and presumably at both sites A and B . If the major Yb sites assume a trivalent state, $|\theta_p|$ should be much smaller because of a sensitive decrease of $|\theta_p|$ with increasing valence, as mentioned above, or else a certain magnetic order or spin glass should appear below $\sim|\theta_p|$. Moreover, the upper limit of the valence at site A is calculated to be 2.87 on the assumption of a divalent state at site B , which again confirms the IV state at site A .

Next, we examined magnetic susceptibilities of $i\text{-AuAlYb}$ and $c\text{-AuAlYb}$ in the lower-temperature region $T \lesssim 100$ K. In both cases, $\chi(T)$'s grow as the temperature decreases. As shown in the insets of Fig. 3, they follow the power law below ~ 20 K; $\chi(T) \propto T^{-0.55}$ for $i\text{-AuAlYb}$ and $\chi(T) \propto T^{-0.42}$ for $c\text{-AuAlYb}$. These results indicate that spin fluctuations develop as temperature decreases to the minimum of 2 K in the both systems. For further lower-temperature region below 2 K, typically three cases are possible. (1) Magnetic order or spin glass occurs. (2) A Fermi-liquid (FL) state appears. In this case, the mass of the electrons should be very heavy. (3) Non-Fermi-liquid (NFL) behavior is observed. The development of the spin fluctuation remains. In order to determine which one is exhibited, we performed specific-heat measurements.

Figure 4(a) shows the temperature dependence of the specific heat of $i\text{-AuAlYb}$ divided by temperature $C(T)/T$.

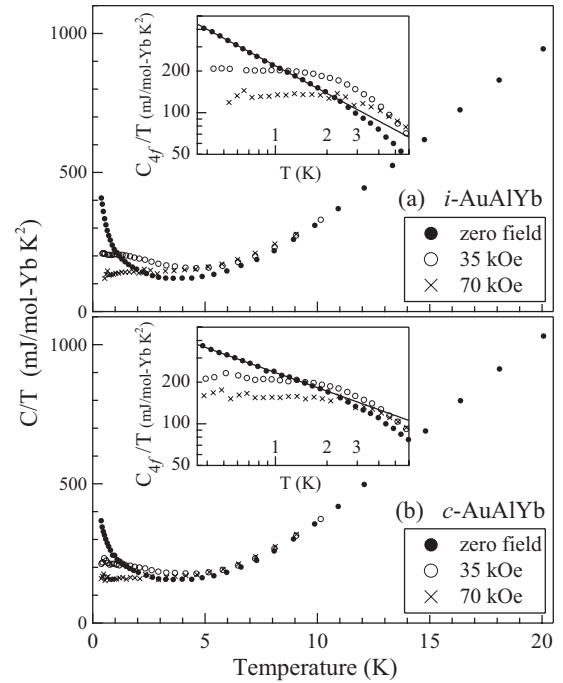


FIG. 4. Specific heat divided by temperature of (a) $i\text{-AuAlYb}$ and (b) $c\text{-AuAlYb}$ as a function of temperature in a zero magnetic field (closed circles), 35-kOe field (open circles), and 70-kOe field (crosses). Insets show the $4f$ electron contribution by logarithm plots. Solid lines are fits to the power law.

The divergent growth of $C(T)/T$ with decreasing temperature in the lowest-temperature region indicates that the spin fluctuations still develop down to 0.38 K. The $4f$ electron contribution $C_{4f}(T)/T$, which was obtained by subtracting the phonon contribution $C_{\text{ph}}(T)/T$, clearly follows the power law; $C_{4f}(T)/T \propto T^{-0.66}$ below ~ 2 K [Fig. 4(a) inset]. Thus, NFL behavior appears in $i\text{-AuAlYb}$ without either doping, pressure, or field tuning as in the case of $\beta\text{-YbAlB}_4$.²⁵ Here, $C_{\text{ph}}(T)$ was estimated by using the Debye model for the low-temperature region βT^3 . The β value was calculated to be 2.79 mJ/mol-Yb K^4 , and the Debye temperature was $\Theta_{\text{D}} = 167$ K, by fitting the equation of $C(T)/T = \gamma + \beta T^2$ to the experimental data between 7–12 K. Additionally, the electrical resistivity $\rho(T)$, measured down to 0.7 K, shows linear temperature dependence; $\rho(T) - \rho_0 \propto T$ below ~ 10 K (ρ_0 : residual resistivity), which is also characteristic of NFL behavior. Combining the observations of the power-law behavior of $\chi(T)$ below ~ 20 K and the linear character of $\rho(T)$ below ~ 10 K, along with taking into account the difficulty of the accurate estimation of $C_{4f}(T)/T$ in the temperature range of several Kelvin or higher, leads us to consider that the NFL character is present below ~ 10 K. In an applied magnetic field, $C(T)/T$ shows temperature-independent behavior in the lowest-temperature region [Fig. 4(a)]. This observation indicates the appearance of a FL state, which would be caused by the suppression of the spin fluctuations under the field. In the FL state for a 35-kOe field, heavy electrons with the electronic specific heat coefficient γ of 200 mJ/mol-Yb K^2 are formed. The onset temperature of the FL behavior is proportional to the applied field such as 1.3 K at 35 kOe and 2.6 K at 70 kOe, which suggests that the NFL behavior appears just in a zero

field. As for the CEF effect, Schottky peaks in the $C(T)/T$ were not observed in the experimental temperature range up to 20 K. The CEF splitting energy Δ_{CEF} is estimated to be more than 65 K because the Schottky peak exhibits a maximum at the temperature $k_{\text{B}}T = 0.31\Delta_{\text{CEF}}$, where k_{B} is the Boltzmann constant. Hence, it is considered that the lowest level of the CEF split states contribute to the NFL behavior. The fact that $\chi(T)$ does not follow the Curie-Weiss fit below ~ 100 K is likely caused by the CEF effect. The temperature scale in this interpretation is consistent with the CEF estimation from the specific-heat measurements.

The NFL behavior also appears in c -AuAlYb. The divergent growth of $C(T)/T$ at the lowest-temperature region is again observed [Fig. 4(b)], and the $C_{4f}(T)/T$ follows a power law: $\propto T^{-0.45}$ [Fig. 4(b) inset]. The obtained Debye temperature $\Theta_{\text{D}} = 168$ K is almost identical to that of i -AuAlYb, which shows their structural similarity. In a magnetic field, the NFL is converted to a FL state, the γ value of which is 210 mJ/mol-Yb K² in a 35-kOe field. Thus, c -AuAlYb exhibits NFL behavior similar to i -AuAlYb. Hence, the Tsai-type atomic clusters that compose both i -AuAlYb and c -AuAlYb would cause the NFL behavior without either doping, pressure, or field tuning. Additionally, the results of the specific heats are consistent with the heterogeneous valence model for i -AuAlYb. In this model, the Yb valence at site A in i -AuAlYb is considered to be close to that of c -AuAlYb, which is responsible for the similar NFL behavior of these two compounds. However, the difference between the two compounds should be noted. The power-law exponent of $C_{4f}(T)/T$ in i -AuAlYb, -0.66 , has a larger magnitude than that in c -AuAlYb of -0.45 , which indicates that i -AuAlYb shows more singularity than c -AuAlYb. The exponent of i -AuAlYb has one of the highest magnitudes among the NFL compounds previously reported. According to the review reports of Refs. 26 and 27, the highest ones are -0.85 and -0.7 for CeRh₂Ga and Ce_{0.1}Y_{0.9}RhIn₅, respectively, but more moderate singularities such as logarithmic divergences are observed in most cases. The difference

of the exponents between i -AuAlYb and c -AuAlYb may be attributed to the difference in the arrangement of the atomic clusters.

In summary, we have found that i -AuAlYb forms an IV quasicrystalline system at ambient pressure. Yb L_3 -edge XANES spectroscopy shows that the mean valence of Yb ions is 2.61. The magnetization measurements demonstrate the localized character of the $4f$ holes in i -AuAlYb, where $\chi(T)$ shows a Curie-Weiss character in the temperature region above ~ 100 K with $\mu_{\text{eff}} = 3.81\mu_{\text{B}}$ per Yb site and $\theta_p = -138$ K. Moreover, c -AuAlYb is also an IV compound with a localized $4f$ character with a higher valence of 2.80 and a larger μ_{eff} of $4.37\mu_{\text{B}}$ than those of i -AuAlYb, but with a similar θ_p of -127 K. As for i -AuAlYb, compared to Yb-based IV crystalline compounds, a valence of 2.61 is rather low for $4f$ -hole localization. To interpret this discrepancy as well as the smaller μ_{eff} in i -AuAlYb, we propose a heterogeneous IV model, which also accounts for the similarity of θ_p between i -AuAlYb and c -AuAlYb. In contrast, c -AuAlYb is a homogeneous IV system. At temperatures below ~ 10 K, NFL behavior appears in both i -AuAlYb and c -AuAlYb without doping, pressure, or field tuning, and $\chi(T)$ and $C_{4f}(T)/T$ exhibit divergent power-law growth as the temperature decreases. In particular, i -AuAlYb shows a strong divergence of $C_{4f}(T)/T \propto T^{-0.66}$ compared to the NFL compounds previously reported.

We thank T. Ishimasa for sample preparation, G. Motoyama and T. Inami for fruitful discussions, K. Kiriyama and H. Kaneko for their technical support, and the Instrument Center of the Institute for Molecular Science for the assistance in the magnetization measurements. This work was performed under Proposals No. 2010A3701 and No. 2010B3701 in BL22XU at SPring-8, and also carried out by the joint research in the Institute for Solid State Physics, the University of Tokyo, and partially supported by a Grant-in-aid for Scientific Research (No. 24540386) from the Japan Society for Promotion of Science.

*wata@spring8.or.jp

[†]Present address: Condensed Matter Research Center, Institute of Materials Structure Science, KEK, Tsukuba, 305-0801, Japan.

[‡]Present address: Faculty of Science and Technology, Tokyo University of Science, Chiba 278-8510, Japan.

[§]Present address: Institute of Multidisciplinary Research for Advanced Material, Tohoku University, Sendai, 980-8577, Japan.

¹J. Flouquet, D. Aoki, F. Bourdarot, F. Hardy, E. Hassinger, G. Knebel, T. D. Matsuda, C. Meingast, C. Paulsen, and V. Taufour, *J. Phys. Conf. Ser.* **273**, 012001 (2011).

²F. Hippert and J. J. Prejean, *Philos. Mag.* **88**, 2175 (2008).

³A. P. Tsai, J. Q. Guo, E. Abe, H. Takakura, and T. J. Sato, *Nature (London)* **408**, 537 (2000).

⁴J. Q. Guo, E. Abe, and A. P. Tsai, *Philos. Mag. Lett.* **82**, 27 (2002).

⁵D. Kawana, T. Watanuki, A. Machida, T. Shobu, K. Aoki, and A. P. Tsai, *Phys. Rev. B* **81**, 220202(R) (2010).

⁶T. Watanuki, D. Kawana, A. Machida, and A. P. Tsai, *J. Phys. Soc. Jpn., Suppl. A* **80** SA087 (2011).

⁷T. Watanuki, D. Kawana, A. Machida, and A. P. Tsai, *Phys. Rev. B* **84**, 054207 (2011).

⁸T. Ishimasa, Y. Tanaka, and S. Kashimoto, *Philos. Mag.* **91**, 4218 (2011).

⁹T. Ishimasa, in *Quasicrystals*, edited by T. Fujiwara and Y. Ishii (Elsevier, Amsterdam, 2008), p. 49.

¹⁰H. Takakura, C. P. Gómez, A. Yamamoto, M. de Boissieu, and A. P. Tsai, *Nat. Mater.* **6**, 58 (2007).

¹¹H. Takakura (private communication).

¹²T. Watanuki, A. Machida, T. Ikeda, A. Ohmura, H. Kaneko, K. Aoki, T. J. Sato, and A. P. Tsai, *Philos. Mag.* **87**, 2905 (2007).

¹³S. Wada and A. Yamamoto, *Phys. B (Amsterdam)* **403**, 1202 (2008).

¹⁴D. T. Adroja, S. K. Malik, B. D. Padalia, and R. Vijayaraghavan, *J. Phys. C: Solid State Phys.* **20**, L307 (1987).

¹⁵E. Bauer, Le Tuan, R. Hauser, E. Gratz, T. Holubar, G. Hilscher, H. Michor, W. Perthold, C. Godart, E. Alleno, and K. Hiebl, *Phys. Rev. B* **52**, 4327 (1995).

- ¹⁶J. Flouquet and H. Harima, arXiv:0910.3110.
- ¹⁷E. Bauer, R. Hauser, L. Keller, P. Fischer, O. Trovarelli, J. G. Sereni, J. J. Rieger, and G. R. Stewart, *Phys. Rev. B* **56**, 711 (1997).
- ¹⁸E. Bauer, R. Hauser, A. Galatanu, H. Michor, G. Hilscher, J. Sereni, M. G. Berisso, P. Pedrazzini, M. Galli, F. Marabelli, and P. Bonville, *Phys. Rev. B* **60**, 1238 (1999).
- ¹⁹K. H. J. Buschow, *Rep. Prog. Phys.* **42**, 1373 (1979).
- ²⁰A. Mitsuda, K. Yamada, M. Sugishima, and H. Wada, *Phys. B (Amsterdam)* **404**, 3002 (2009).
- ²¹J. M. Lawrence, G. H. Kwei, P. C. Canfield, J. G. DeWitt, and A. C. Lawson, *Phys. Rev. B* **49**, 1627 (1994).
- ²²B. C. Sales and D. K. Wohlleben, *Phys. Rev. Lett.* **35**, 1240 (1975).
- ²³Ö. Rapp, in *Physical Properties of Quasicrystals*, edited by Z. M. Stadnik (Springer, Berlin, 1999), p. 127.
- ²⁴Y. Muro, K. Yamane, M. S. Kim, T. Takabatake, C. Godart, and P. Rogl, *J. Phys. Soc. Jpn.* **72**, 1745 (2003).
- ²⁵S. Nakatsuji, K. Kuga, Y. Machida, T. Tayama, T. Sakakibara, Y. Karaki, H. Ishimoto, S. Yonezawa, Y. Maeno, E. Pearson, G. G. Lonzarich, L. Balicas, H. Lee, and Z. Fisk, *Nat. Phys.* **4**, 603 (2008).
- ²⁶G. R. Stewart, *Rev. Mod. Phys.* **73**, 797 (2001).
- ²⁷G. R. Stewart, *Rev. Mod. Phys.* **78**, 743 (2006).